Multi-scale Discrete Dislocation Plasticity Analysis: Application to Nano-indentation

Shafique M. A. Khan* and Lyle E. Levine**

Materials Science and Engineering Laboratory
National Institute of Standards and Technology, Gaithersburg, MD, USA
*shafique.khan@nist.gov
**lyle.levine@nist.gov

ABSTRACT

To closely analyze the dislocation structure evolution during nano-indentation, a multi-scale discrete dislocation plasticity code is modified to include nano-indentation loading. This code couples two length scales, discrete dislocation dynamics and continuum finite element analysis and has been successfully applied to analyze various problems in mechanics and materials science. Description of the multi-scale code is presented; followed by the methodology to implement nano-indentation loading in the model. The numerical accuracy of the new model is investigated and shown to be excellent for small contact area between indenter tip and the specimen. Representative results are shown for dislocation structure evolution during nano-indentation.

Keywords: nano-indentation, multi-scale, dislocation dynamics, plasticity, dislocation structure

1 INTRODUCTION

With the growing use of nano-scale components in various technologies like MEMS, NEMS, thin films, medical diagnostics etc., nano-indentation testing is finding new, expanding applications towards quantitative determination of mechanical properties at the nano-scale. In addition, it represents a 'non-destructive' testing technique for macro applications, since mechanical properties of the bulk material can be extracted from nano-indentation testing using appropriate models. Thus, accurate models of the nano-indentation process are crucial at various length scales.

3D discrete dislocation dynamics is a computational tool developed to simulate and track the evolution of large dislocation structures (much larger than an atomistic simulation can handle) during deformation. It also provides the crucial length scale for bridging the atomistic length scale to the continuum length scale for various applications including nano-indentation. When 3D discrete dislocation dynamics is coupled with continuum finite element analysis, the result is a 3D Multi-scale Discrete Dislocation Plasticity model (*MDDP*), in which finite element analysis is responsible for applying the model boundary conditions and tracking the shape changes, whereas discrete dislocation dynamics is responsible for the dislocation motion/evolution. *MDDP* has been applied to investigate various problems e.g., monotonic loading, dislocation boundaries, impact loading[1].

In the present study, we develop and incorporate the model for nano-indentation into *MDDP*. The study validates the developed model and analyzes the dislocation structure evolution during nano-indentation. Since dislocation dynamics tracks the evolving dislocation microstructure, this model provides a tool that incorporates the effect of the dislocation microstructure directly into larger length scales.

2 MULTI-SCALE DISCRETE DISLOCATION PLASTICITY

In dislocation dynamics (*DD*) simulations, the plastic deformation of a single crystal is modeled by explicitly accounting for the evolution of a multitude of dislocation loops and curves. The dislocations are discretized into straight line-segments of mixed character. The Peach-Koehler force acting on a dislocation segment is calculated from the stress field of all other dislocations and the applied stress. For a dislocation segment bounded by j and $j+1$, the Peach Koehler force $\mathbf{F}_{j,j+1}$ on the segment is obtained by integration over the entire segment length L, such that:

$$\mathbf{F}_{j,j+1} = \left(\sum_{i=1}^{N-1} \frac{1}{L} \int_{L} \left(\sigma^{D}_{i,i+1}(p) + \sigma^{a}(p) \right) \cdot \mathbf{b}_{j,j+1} \right) \times \boldsymbol{\xi}_{j,j+1} \mathrm{d}l + \mathbf{F}_{j,j+1-self} \quad (1)$$

where p is a field point on the dislocation segment $j,j+1$, N is the total number of nodes, $\sigma^{D}_{i,i+1}(p)$ is the stress from a remote dislocation segment bounded by i and $i+1$, $\sigma^{a}(p)$ is any other externally applied stress plus internal friction (if any) and the stress induced by other defects, $\mathbf{b}_{j,j+1}$ is the Burgers vector, $\boldsymbol{\xi}_{j,j+1}$ is the line sense vector, and $\mathbf{F}_{j,j+1\text{-}self}$ is the Peach Koehler force corresponding to local interaction between the dislocation segment adjacent to $j,j+1$. Then, following the standard finite element procedure and using the linear interpolation shape functions over the segment, the Peach Koehler force per unit length $\mathbf{F}_{j,j+1}$ is distributed equally to the nodes j and $j+1$. Thus, once all the

forces are assembled, the net force on each node has contributions from all the segments connected to it. The N dislocation nodes move simultaneously in the glide direction over a characteristic time corresponding to the least time increment required for an interaction to take place. The governing equation of glide motion for each dislocation node is nonlinear and given as:

$$m_i^* \dot{\boldsymbol{v}}_i + \frac{1}{\mathrm{M}_i(\mathrm{T},\mathrm{P})} \boldsymbol{v}_i = \mathbf{F}_{i\ glide-component} \tag{2}$$

where m_i^* is the effective mass per unit dislocation length, M_i is the dislocation mobility which could depend on both temperature T and pressure P, $\boldsymbol{v}_i$ is the velocity of node i, $\dot{\boldsymbol{v}}_i$ is the acceleration, and $\mathbf{F}_{i\ glide-component}$ is the glide component of the Peach-Koehler force. Thus, the motion and interaction of an ensemble of dislocations in a 3-D crystal is integrated over time yielding macroscopic plastic distortion, the rate of which is defined as:

$$\dot{\boldsymbol{\varepsilon}}^{\mathrm{p}} = \sum_{i=1}^{\mathrm{K}} \frac{l_i v_{gi}}{2\,\mathrm{V}} (\mathbf{n}_i \otimes \mathbf{b}_i + \mathbf{b}_i \otimes \mathbf{n}_i) \tag{3}$$

where l_i is the segment length, $\mathbf{n}_i$ is a unit normal to the slip plane, v_{gi} is the magnitude of the glide velocity, K is the total number of segments and V is the volume of the representative volume element (*RVE*). For details of the *DD* code that is used in this study, see ref. [2-4].

Using *DD* for infinite domain problems, the computational cell as a whole is considered as a representative volume element, with either reflection boundary conditions (ensuring the continuity of the dislocation curve) or periodic boundary conditions (ensuring conservation of the dislocation flux across boundaries as well as continuity). However, for the simulation of unit cells representing grain boundaries or for finite domain problems, these models are no longer valid, and a more rigorous treatment of boundary conditions is required. This issue has recently been addressed by Zbib and co-workers [1,5-7] by developing the *MDDP* model that couples the micro-scale *DD* with the continuum scale finite element analysis (FEA). In this method, the dislocations contained within the representative volume element (*RVE*) are treated as an internal stress $\mathbf{S}^{\mathbf{D}}$ (homogenized over the element), and the effective total stress within the *RVE* is the sum of the stresses by all external agencies and the internal stress $\mathbf{S}^{\mathbf{D}}$. With this approach, one can deal with mixed boundary conditions of cells containing complex dislocation structures.

3 NANO-INDENTATION MODELING

MDDP is developed as a computational tool to study the behavior of dislocations under different types of loads and it must be first modified to include the nano-indentation loading. Careful literature review of the models used to simulate nano-indentation outlines two possible approaches that can be used in *MDDP*. The first approach is to include the indenter in the simulations as a separate entity; the nano-indentation simulations can be performed by applying a load to the indenter, forcing it against the top surface of the specimen. The second approach is to model the effect of the loaded indenter on the top surface of the specimen without including the indenter in the simulations. With current capability of *MDDP* (cubic cells for *DD* and superimposed brick elements for FEA), the first option presents a modeling problem where we need to generate additional finite elements of various geometries, together with new meshing algorithms. The second option provides an effective alternate with good numerical accuracy when properly employed. Therefore, the effect of the loaded indenter will be modeled in this study, and the effectiveness and accuracy of this approach will be investigated.

3.1 Hertz Contact Theory

The loaded indenter exerts a force on the specimen surface, which can be determined using the theory of contact mechanics. Of the various contact mechanics theories available, Hertz theory [8-10] will be used, as it is frequently confirmed by the experimental observations. For a spherical indenter, Hertz theory relates radius of the contact circle, 'a' (between indenter and specimen) to the indenter load P as:

$$\mathrm{a}^3 = \frac{3\mathrm{PR}}{4\mathrm{E}^*} \tag{4}$$

where R is the radius of indenter tip and E^* is the reduced or combined modulus for the indenter and specimen materials. The pressure distribution for a spherical indenter is:

$$\mathrm{p_s} = \frac{3}{2}\frac{\mathrm{P}}{\pi \mathrm{a}^2}\left(1 - \left(\frac{\mathrm{r}}{\mathrm{a}}\right)^2\right)^{1/2} \tag{5}$$

The isosurfaces of $\mathrm{p_s}$ have the shape of a half ellipsoid under the contact area circle.

3.2 Implementation in *MDDP*

Equations 4 and 5 can be used to convert the indenter load to a distributed load over the specimen/simulation cell top surface in *MDDP*. As cubic cells/brick elements are used in *MDDP*, there is a restriction on both the size and shape of the contact area that can be used. Therefore, in *MDDP* the controlling factor is the contact area, and this is incremented during simulation rather than the indenter load. In addition, since the shape of the contact area is always non-circular (a shape with straight sides due to the use of cubic cells/elements in *MDDP*), the pressure distribution

obtained for a circular contact area with radius 'a' must be translated for a non-circular contact area of best fit. In here, we propose to use a square contact area so that the theoretical half ellipsoidal pressure distribution is approximated by a cube with an equivalent uniform pressure $p_{s,eq}$, giving the following relation:

$$p_{s,eq} = \frac{2}{3}\frac{\pi a^2 p_{s,max}}{b^2} \qquad (6)$$

where $p_{s,max}$ is the maximum theoretical pressure directly below the indenter tip. Based on this equation, the circular contact area is approximated by a square contact area of side *b* and the contact area increases from 1x1 element to 3x3 elements and then to 5x5 elements and so on.

4 RESULTS AND DISCUSSION

The corresponding equivalent load can be calculated from the equivalent pressure as obtained from Eq. 6. The equivalent load is then uniformly distributed over the square contact area. Initial simulations, however, showed that the equivalent load must be applied non-uniformly over the square contact area. The resulting load distribution in *MDDP* along with the theoretical ellipsoidal distribution is shown in Fig. 1.

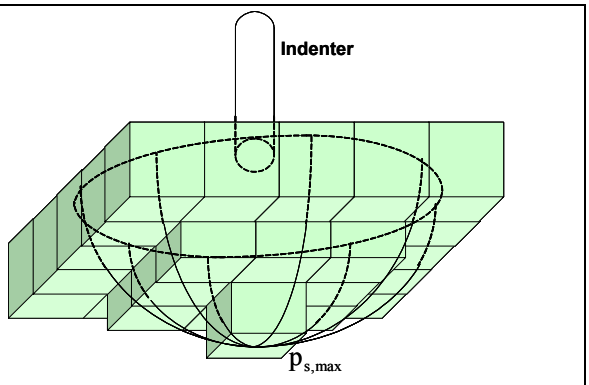

Figure 1: Qualitative representation of the indenter pressure distribution, in-plane dimensions are of length and out of plane dimension is of pressure (Dotted lines shows the theoretical pressure distribution)

The above analysis is presented for a spherical indenter tip; however it could be extended to other indenter tip shapes using appropriate geometrical approximations. Currently, *MDDP* can simulate spherical and Berkovich indenters. We will use the theoretical values from Hertz's relations for comparison to assess the computational accuracy of the nanoindentation model.

Figure 2a shows the load-maximum displacement plot for a spherical indenter of radius R = 230 nm. The indenter is assumed rigid and the shear modulus used for the Gold specimen is 27 GPa. The *MDDP* nanoindentation model matches well with the theoretical values up to 7x7 (49 elements) contact area. The same is true for the Berkovich indenter. This is explained by noting that the approximation of circular contact area by a square area is not accurate for more than 7x7 elements size. It is determined that this does not depend on finite element mesh size but only on the number of finite elements used to approximate the contact area. For a contact area with more than 7x7 elements, a more aggressive algorithm is needed for a more accurate approximation. The second reason for this deviation is that the Hertz theory is not valid for large contact area as compared to the indenter radius. Figure 2b shows the displacement profile under the indenter tip and across the top surface of the simulation cell. Theoretical curves are plotted only to the extent of the contact area as Hertz theory is not valid outside the contact area. The results are very encouraging up to 5x5 (25 elements) size.

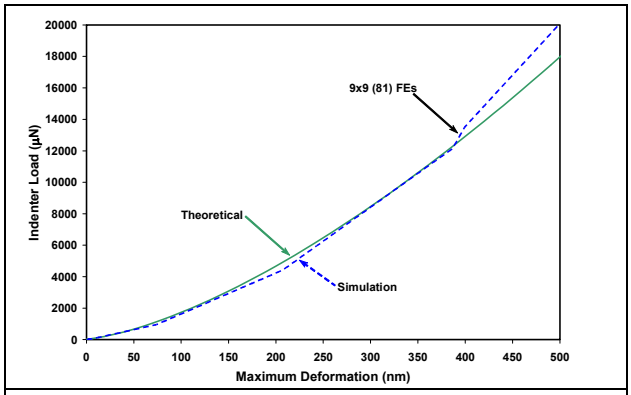

Figure 2a: Load displacement plot: Spherical indenter

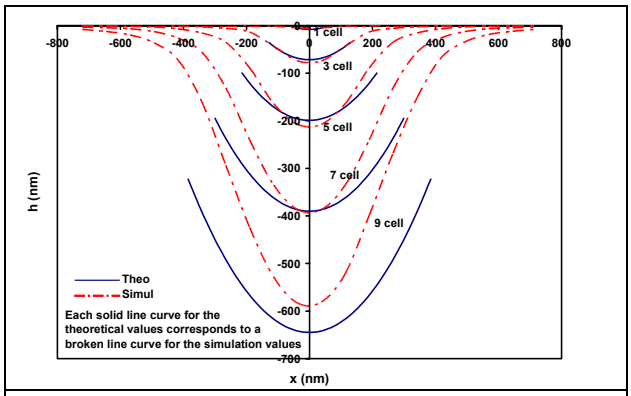

Figure 2b: Displacement profile: Spherical indenter

All of the results presented to this point are performed without any dislocations in the simulation cell to check the accuracy of the nano-indentation model. In order to investigate the effect of dislocations, random pairs of Frank-Read sources are placed in the *RVE*. Then several simulations are carried out to observe the behavior of dislocations in the simulation cell. The indenter load is applied up to 3x3 elements. Representative results are shown in Fig. 3a (Berkovich indenter, with semi angle of 65.3°), which shows the random initial dislocation structure

and the evolved dislocation microstructure. As expected, most of the dislocation movement and generation takes place directly below the indenter tip (center of the top surface). The thick (red) lines show the 'escaped' dislocations from the top surface, which are largely responsible for the final shape of the loaded top surface under nano-indentation. This pattern of slip lines is consistent with atomic force microscopy observations of nano-indentation of fcc metals[11]. The load-displacement plot in Fig. 3b includes the new curve with dislocations present, which shows the plastic deformation after complete unloading due to the dislocation activity. The curve without any dislocations present, shown for comparison, is the same for both loading and unloading.

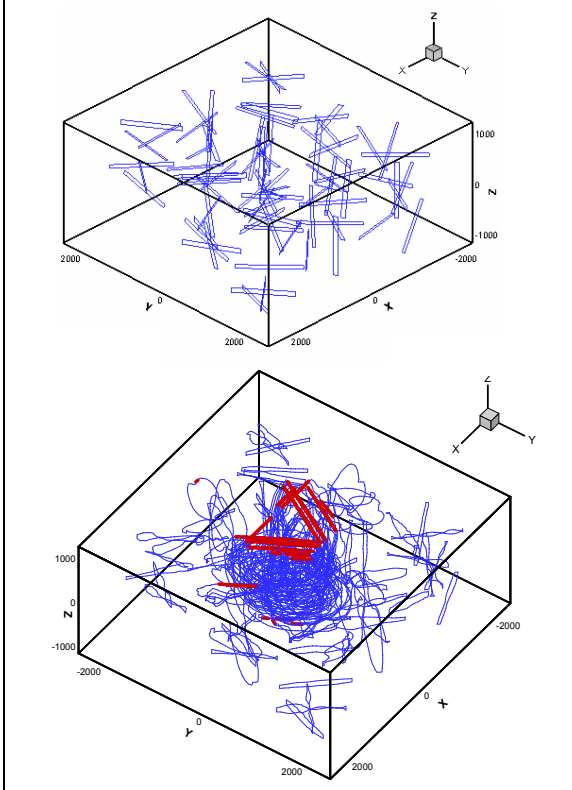

Figure 3a: Dislocation evolution: Berkovich indenter
Initial and evolved dislocation structures
(Thick (red) lines show the escaped dislocations, units are in Burgers vector)

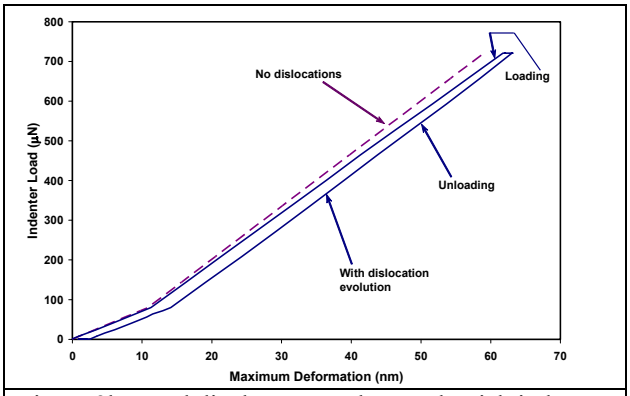

Figure 3b: Load displacement plot: Berkovich indenter, Effect of dislocation evolution

REFERENCES

[1] Zbib, H.M., Shehadeh, M., Khan, S.M.A., and Karami, G., "Multiscale Dislocation Dynamics Plasticity", Int. J. Multiscale Comp. Eng., 1(1), 73-89, 2003.

[2] Zbib, H.M., Rhee, M., Hirth, J.P., "3-D simulation of curved dislocations: discretization and long range interactions", In: Advances in Engineering Plasticity and its Applications, Abe and Tusta, T., (Eds), Elsevier Science Ltd, NY, 15-20, 1996.

[3] Zbib, H.M., Rhee, M., Hirth, J.P., "On plastic deformation and the dynamics of 3D dislocations", Int. J. Mech. Sci. 40, 113-127, 1998.

[4] Rhee, M., Zbib, H.M., Hirth, J.P., Huang, H., de La Rubia, T.D., "Models for long-/short-range interactions and cross slip in 3D dislocation simulation of BCC single crystals", Modeling and Simulations in Maters. Sci. & Eng. 6, 467-492, 1998.

[5] Yasin, H., Zbib, H.M., Khaleel, M.A., "Size and boundary effects in discrete dislocation dynamics: coupling with continuum finite element", Mater. Sci. Eng., A309-310, 294-299, 2001.

[6] Zbib, H.M., de La Rubia, T.D., "A multiscale model of plasticity", Int. J. Plasticity 18, 1133-1163, 2002.

[7] Khan, S.M.A., Zbib, H.M., and Hughes, D.A., "Modeling Planar Dislocations Boundaries using Multi-scale Dislocation Dynamics Plasticity", Int. J. Plasticity, 20, 1059-1092, 2004.

[8] Timoshenko, S., "Theory of Elasticity", McGraw-Hill, 1934.

[9] Johnson, K.L., "Contact Mechanics", Cambridge University Press, 1985.

[10] Fischer-Cripps, A.C., "Nanoindentation", Springer-Verlag NY Inc., 2002

[11] Nibur, K.A., and Bahr, D., "Identifying slip systems around indentations in FCC metals", Scripta Mater., 49, 1055-1060, 2003.